Laser nanosurgery of single microtubules reveals location-dependent depolymerization rates

Nicole M. Wakida
Christopher S. Lee
Elliot T. Botvinick
University of California at Irvine
Beckman Laser Institute
Irvine, California 92612
E-mail: nwakida@uci.edu

Linda Z. Shi
University of California at San Diego
Department of Bioengineering
La Jolla, California 92093-0435

Alexander Dvornikov
Michael W. Berns
University of California at Irvine
Beckman Laser Institute
Irvine, California 92612

Abstract. In this study, 532-nm picosecond and 800-nm femtosecond lasers are used in combination with fluorescently labeled tubulin to further elucidate microtubule depolymerization and the effect lasers may have on the resulting depolymerization. Depolymerization rates of targeted single microtubules are dependent on location with respect to the nucleus. Microtubules located near the nucleus exhibit a significantly faster depolymerization rate when compared to microtubule depolymerization rates near the periphery of the cell. Microtubules cut with the femtosecond laser depolymerize at a slower rate than unirradiated controls ($p=0.002$), whereas those cut with the picosecond laser depolymerize at the same rate as unirradiated controls ($p=0.704$). Our results demonstrate the ability of both the picosecond and femtosecond lasers to cut individual microtubules. The differences between the two ablation results are discussed. [DOI: 10.1117/1.2718920]

Keywords: laser nanosurgery; microtubule; depolymerization.

Paper 06261RR received Sep. 19, 2006; revised manuscript received Dec. 21, 2006; accepted for publication Dec. 22, 2006; published online Apr. 24, 2007.

1 Introduction

In this study, picosecond and femtosecond laser systems are used in combination with a tubulin cyan fusion protein (CFP) to elucidate the dynamics of single microtubules in living cells. This study further considers the suggestion that ultrashort femtosecond laser pulses produce a more precise ablation zone.[1]

Near-infrared femtosecond lasers were first used by Konig and Riemann for cellular nanosurgery to ablate regions within the nucleus of Chinese hamster ovary (CHO) cells.[2] Further work demonstrated the ability of femtosecond laser pulses to produce regions of damage 100 to 200 nm in diameter in extracellular isolated and dried chromosomes. This was well below the diffraction limit for the focused 800-nm laser.[3] Other studies utilizing femtosecond lasers as nanoscale ablation tools include targeting of mitochondria,[4] mitotic spindles in yeast,[5] single microtubules,[1] and single stress fibers.[6]

It has been suggested that with its short pulse duration, femtosecond lasers are capable of efficient ablation dependent on plasma formation by multiphoton absorption and ionization. This is due to the lower energy threshold for optical breakdown as compared to longer pulsed lasers. Thus under optimal conditions, it is thought that femtosecond laser ablation events are confined only within the focal point of the laser.[7]

Of particular interest is the claim that femtosecond lasers are superior to other pulsed laser systems for the nanosurgery of cells.[1] There is sufficient literature demonstrating that nanosecond 532-nm,[8–11] picosecond UV 355-nm,[12] nanosecond UV 266-nm,[13] picosecond 532-nm,[14] and nonlaser continuous wave UV[1,13,15,16] sources can all be used for subcellular surgery, especially as related to cytoskeletal microtubules and cell division.

We demonstrate that both the near-IR femtosecond laser and the picosecond frequency-doubled 532-nm Nd:YAG laser can ablate submicron regions of single microtubules in living cells. Furthermore, our microtubule dynamics experiments demonstrate that depolymerization rates of single laser-cut microtubules are faster for microtubules located above or below the nucleus, as opposed to those located in the peripheral cytoplasm. These results are discussed with respect to other laser nanosurgery studies on microtubules as well as the extensive literature on nonlaser UV microbeam irradiation of microtubules, and observations on microtubule growth and shrinkage rates in nonirradiated cells.

2 Results

2.1 *Single Cyan Fusion Protein Microtubule Cutting*

It was possible to cut single microtubules with the femtosecond laser and determine the postirradiation rate of depolymerization for up to sixty seconds following the laser exposure [Figs. 1(a)–1(h)]. Depolymerization was defined as a decrease in the length of the microtubules, as tubulin monomers are released from the ends of the microtubule polymers. Varying depolymerization rates were observed within the microtubule population, as depicted by the difference in microtubule depolymerization between Figs. 1(a)–1(d) and Figs. 1(d)–1(h).

By varying laser irradiance (W/cm^2) distinct categories of microtubule responses and their threshold values were observed (Table 1 and Fig. 2). First, immediate depolymeriza-

Address all correspondence to Nicole Wakida, Beckman Laser Institute, University of Calilfornia, Irvine 1002 Heath Science Rd- Irvine, CA 92612 United States of America; Tel: 949–824–9703; Fax: 949–824–8413; E-mail: nwakida@uci.edu

1083-3668/2007/12(2)/024022/8/$25.00 © 2007 SPIE

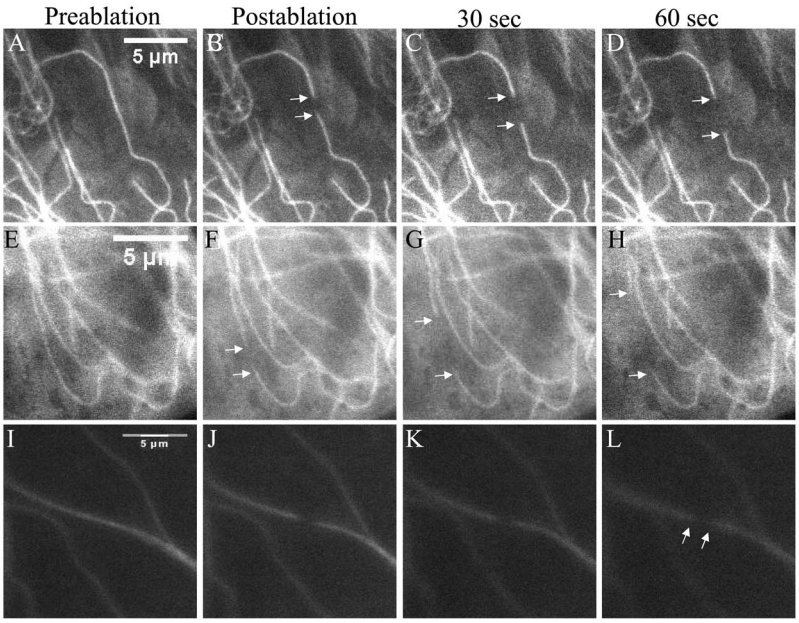

Fig. 1 Laser exposure and effects on single microtubules. (a), (e), and (i) Fluorescence images before laser exposure. (b), (f), and (j) Images captured immediately after laser exposure show a loss of fluorescence in the targeted region. (c), (d), (g), and (h) Time periods of 30 and 60 s following laser exposure above irradiance and energy levels of 25.6×10^5 W/cm^2; note changes in the targeted microtubule length by depolymerization. (k), and (l) At time periods of 30- and 60-s postlaser exposures with irradiance and energy levels below 20×10^5 W/cm^2; note no subsequent depolymerization follows laser exposure.

tion of the targeted microtubule occurred at an irradiance of 24×10^5 W/cm^2 where three of eight (40%) irradiated microtubules depolymerized. When the irradiance was reduced to 20×10^5 W/cm^2 one of ten (10%) depolymerized. An increase in Irradiance to 26×10^5 W/cm^2 always resulted in microtubule depolymerization [Figs. 1(a)–1(h)]. Second, a loss in fluorescence at the targeted region with no subsequent depolymerization following laser exposure was indicative of photobleaching of the fluorescent CFP molecule [Figs. 1(i)–1(l)] (see tubulin antibody staining in next section). Photobleaching of the targeted microtubule was consistently observed between irradiance levels of 12×10^5 and 20×10^5 W/cm^2. To confirm this threshold value, the irradiance was decreased to 8×10^5 and 4×10^5 W/cm^2, where no change in microtubule fluorescence was detected. (Fig. 2). Thus, under the conditions of this study, the photobleaching threshold is between 12×10^5 and 20×10^5 W/cm^2.

Table 1 Irradiance and energy density values for photobleaching and cutting thresholds by the femtosecond laser. Settings below the photobleaching thresholds result in no change to the targeted microtubule. At the cutting threshold, 50% of targeted microtubules are successfully ablated. Settings above the supra-cutting threshold always result in successful ablation of the targeted microtubule.

Irradiance (W/cm^2)	Energy density (J/cm^2)	Threshold
20×10^5	3.0×10^4	Photobleaching
24×10^5	3.6×10^5	Ablation
26×10^5	4×10^5	Supra-ablation

2.2 *Immunofluorescence of Cut Cyan Fusion Protein Microtubules*

To determine if a loss of fluorescence was indicative of microtubule cleavage as opposed to photobleaching, single irradiated microtubules were fixed and stained with fluorescently conjugated antibodies to tubulin immediately following laser exposure. Figure 3 compares a photobleached microtubule

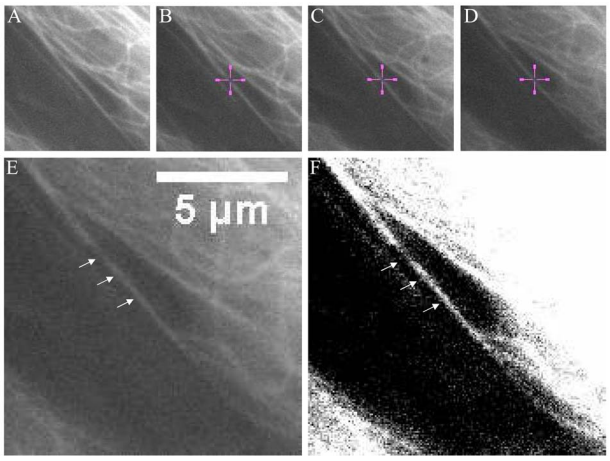

Fig. 2 Irradiation of a microtubule bundle at irradiance levels below ablation threshold. (a) Image prior to laser exposure. (b), (c), (d) Crosshairs depict exact location of laser exposure for 12×10^5, 8×10^5, and 4×10^5 W/cm^2. (e) Image following ablation shows a slight loss in fluorescence in the region corresponding to the 12×10^5 W/cm^2. (f) A contrast-enhanced image clearly shows a change in fluorescence at 12×10^5 W/cm^2 but no effect on fluorescence for 8×10^5 W/cm^2 or below.

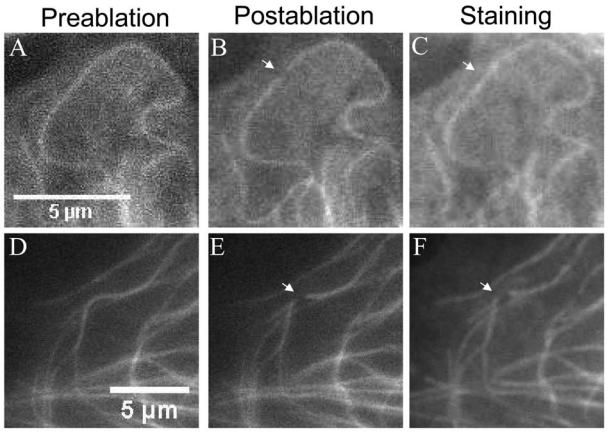

Fig. 3 Single irradiated microtubules at different laser exposure parameters resulting in an absence or presence of immunofluorescence staining. (a) and (d) Prelaser exposure images of single microtubules. (b) and (e) Images immediately after laser exposure, demonstrating a loss in fluorescence at the targeted region. Immunofluorescence staining shows the presence of staining at 6.7×10^5 W/cm^2, but an absence of staining (c) at 26×10^5 W/cm^2. (f) Loss of staining confirms a successful ablation event.

[Figs. 3(a)–3(c)] and a cleaved microtubule [Figs. 3(d)–3(f)]. For the photobleached microtubule, there was a loss of tubulin fluorescence immediately after irradiation, but positive tubulin immunofluorescence staining in the irradiated region. For the cleaved microtubule, the 0.47 μm diameter cut exhibited a loss of fluorescence immediately following irradiation, and immuno-stained negatively in that region [Figs. 3(d)–3(f)]

2.3 *Microtubules Dynamics*

2.3.1 *Femtosecond cutting of cyan fusion protein microtubules*

Depolymerization rates were calculated for newly formed plus ends of cut microtubules and for control nonablated microtubules that were observed to depolymerize spontaneously. Figure 4 illustrates depolymerization of both cut microtubules and control microtubules in the same region of a cell. The mean rate of induced plus end depolymerization was 3.54 ± 3.14 μm/min, while the mean rate of spontaneous depolymerization of noncut control microtubules was 5.78 ± 4.50 μm/min (Fig. 5). Using a rank-sum statistical test, it was determined that new plus ends created by laser cutting depolymerized at rates slower than the rates of spontaneously depolymerizing microtubules ($p=0.002$).

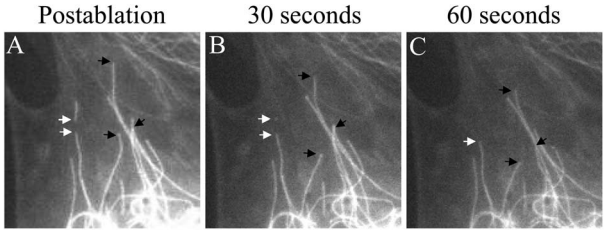

Fig. 4 Depolymerization of a single microtubule (white) following laser cutting observed among untargeted, control microtubules (black). Depolymerization rates were calculated for microtubules in the adjacent nonlaser-exposed region over a 60-s time period.

2.3.2 *Picosecond cutting of cyan fusion protein microtubules*

To determine if the pulse duration or wavelength of the laser had an effect on the depolymerization rates at plus ends, a picosecond laser emitting at 532 nm was used to ablate CFP microtubules. The average rate of depolymerization for ablated plus ends was 3.95 ± 2.54 μm/min and 3.72 ± 1.84 μm/min for control microtubules (Fig. 5). There was no significant difference between cut and control depolymerization rates ($p=0.704$).

To determine if the position of the microtubule with respect to the nucleus had an effect on microtubule depolymerization rates, single microtubules residing above or below the nucleus were targeted with the picosecond laser (Fig. 6). The average rate for plus end depolymerization was 13.66 ± 8.84 μm/min [Fig. 5(d)]. Plus-end depolymerization rates above or below the nucleus were significantly different ($p\ll0.01$) than microtubules cut at the periphery of the cell (3.54 ± 3.14 μm/min).

3 Discussion

We have demonstrated that a near-IR (800 nm) femtosecond laser can be used to perform precise subcellular nanosurgery on individual microtubules in live cells. Severed microtubules can be followed and analyzed with respect to depolymerization (shrinkage) dynamics. However, when compared to the 532-nm picosecond Nd:YAG laser,[14] the 532-nm nanosecond laser,[8] and the 355-nm picosecond Nd:YAG laser,[12] we find that there is no significant advantage of the femtosecond laser, and there may, in fact, be some disadvantages.

It is noteworthy that the average rates of depolymerization after the 800-nm femtosecond laser cuts were different from the control noncut depolymerization rates ($p=0.002$), whereas there was no difference in the average rates of depolymerization between the 532-nm picosecond-cut microtubules and the depolymerization rates of nonirradiated control microtubules ($p=0.704$) (Fig. 5). The shorter pulse femtosecond laser had a peak irradiance of 157 GW/cm^2 in the focused spot, whereas the picosecond laser had a peak irradiance of 7 GW/cm^2 (Table 2). This twenty-fold difference in peak irradiance could have played a role in the observed differences between the picosecond and femtosecond laser effects on microtubule depolymerization rates. Calculations in a previous picosecond laser study[14] strongly suggested a multiphoton-induced ionization and plasma formation mechanism of ablation. It is likely that similar mechanisms are occurring in the femtosecond laser ablations reported here. This would be consistent with other femtosecond laser studies.[3,7] However, the difference in the depolymerization rates following exposure to the two lasers bears further examination with respect to biological and physical mechanisms.

Fluorescent images from postirradiation and immunofluorescence staining revealed an ablation diameter of 0.47 μm, which is smaller than the 0.7-μm calculated focal spot of the laser (see Sec. 4). To determine the ability of the femtosecond laser to make precise cuts in cellular structures within living cells, EM analysis of picosecond ablations demonstrated its

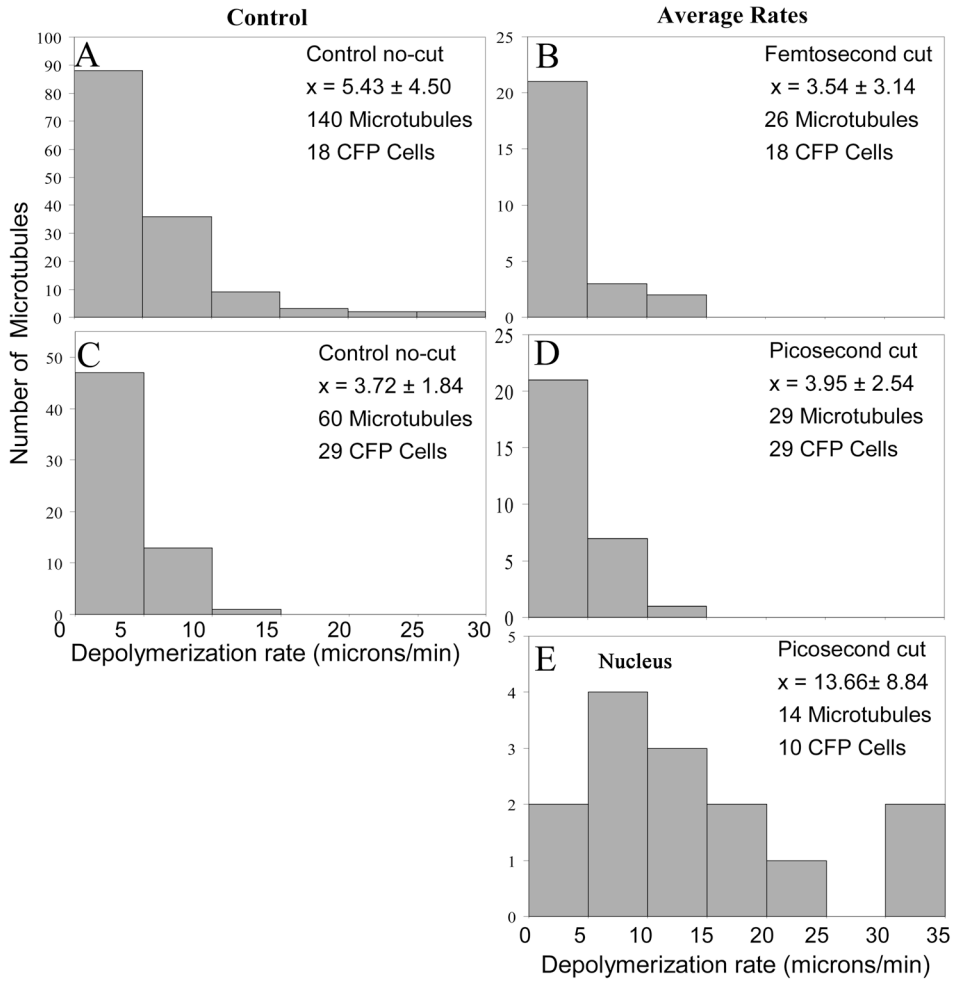

Fig. 5 Distribution of depolymerization rates for control microtubules and newly formed plus ends. (a) and (c) Distribution of mean depolymerization rates of untargeted, control microtubules. (b), (d), and (e) Distribution of mean depolymerization rates of newly formed plus ends of microtubules resulting from laser irradiation. Two data sets (a) and (c) represent varying experimental conditions between experiments with the same call line. Data correspond to experiments targeting (a) and (d) CFP-tubulin with the femtosecond laser, (c) and (b) CFP tubulin with the picosecond laser, and (e) CFP-tubulin microtubules residing near the nucleus ablated with the picosecond laser. Each histogram includes information about the parameters, mean depolymerization rate, number of microtubules, and number of cells observed.

ability to ablate regions 0.34 μm in diameter, which was below the 0.47-μm focal diameter of the laser.[14] Thus both laser systems appear to be able to ablate regions of cellular structure less than the theoretical size of the laser focal point. This may be due to the fact that a Gaussian profile laser beam is focused to a Gaussian focal spot, which may be above lesion threshold only at the center of the Gaussian.[17,18]

Our results on microtubule depolymerization following cutting must be viewed in the context of the many published *in-vitro* (test tube) and *in vivo* (live cell) studies on single microtubule dynamics. First, we have determined the ablation (cutting) threshold for individual microtubules. (Table 1). This is important both for repeatability by other investigators as well as for understanding the physical mechanism(s) of the ablation process.[14,18] Furthermore, a loss of fluorescence in the irradiated region of a microtubule may be due either to photobleaching of the fluorescent fusion protein (CFP, YFP, GFP, etc.), or to an actual ablation/cut of the microtubule. Thus it was important to fix and stain cells with fluorescent antitubulin and relocate the irradiated microtubule (Fig. 3). In

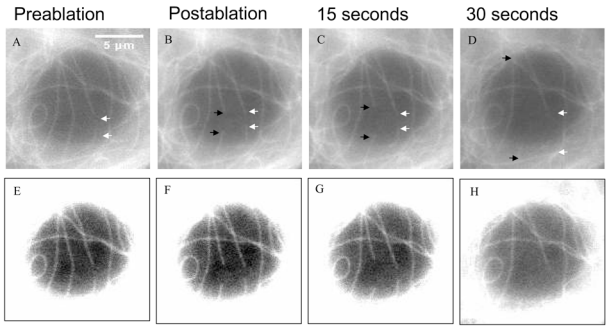

Fig. 6 Laser irradiation of microtubules positioned near the microtubule organizing center, above or below the nucleus. (a) Preablation image compared to (b) post ablation image reveals the location of the target prior to laser exposure. (c) 15 s and (d) 30 s after ablation, showing the depolymerization of the targeted microtubule (black arrows). Depolymerization of a previously ablated microtubule in the same field of view (white arrows). (e) through (h) Contrast-enhanced images clearly showing the depolymerization of microtubules across the nucleus region.

Table 2 Comparison of laser parameters for femtosecond and picosecond laser cutting thresholds of CFP tubulin in PtK2 cells.

	Femtosecond laser	Picosecond laser
Repetition rate	76 MHz	76 MHz
Pulse duration	200 fs	80 ps
Wavelength	800 nm	532 nm
Focused spot diameter (from 1.22 l/NA)	0.7 mm	0.46 mm
Focused spot area	3.82×10^{-9} cm^2	1.66×10^{-9} cm^2
Energy per pulse	0.11 nJ	0.92 nJ
Peak irradiance	157 GW/cm^2	7 GW/cm^2
Exposure time (average irradiance)	150 ms	3 ms
Deposited energy/area (energy density)	3.6×10^5 J/cm^2	1.24×10^5 J/cm^2
Average irradiance	2.4×10^6 W/cm^2	4.1×10^7 W/cm^2

this way ablation thresholds were determined. The ablation threshold for the femtosecond laser was 2.4×10^6 W/cm^2, while for the picosecond laser it was 4.1×10^7 W/cm^2, a twenty-fold difference in average irradiance but with only a three-fold difference in fluence (Table 2).[14,18]

Second, the individual microtubule depolymerization rates for most of the experiments reported here were generally less than those reported in the literature, whether for laser-cutting experiments, classic nonlaser UV cutting, or noncutting experiments where control shrinkage rates were determined. For example, Colombelli et al.[12] reported an average shrinkage rate of 19.5 μm/min for individual YFP-transfected microtubules in PtK2 cells severed with the 355-nm picosecond UV laser. In nonlaser UV cutting of the plus ends of microtubules *in vitro*, an average shortening rate of 21 μm/min[15] was measured in one study and 22 μm/min was reported in another study.[19] Similarly in PtK2 and LLCPK cells, Rusan et al.[20] reported shrinkage rates for nonsevered microtubules of 14.8 and 13.1 μm/min for rhodamine tubulin and eGFP transfected tubulin, respectively. Also, Shelden and Wadsworth[21] measured shrinkage rates of 19.8 μm/min for PtK1 cells and 32.2 μm/min in Chinese hamster ovary (CHO) cells. In *Taricha granulosa* newt lung cells, average shortening rates of 17.3 μm/min were measured,[22] and in the South African clawed toad *Xenopus laevis*, average shortening rates were 12.8 μm/min.[23] Slower average shrinkage rates of 7.4 μm/min were measured in PtK1 cells,[24] and 4.3 μm/min in human neonatal fibroblasts.[25] The shrinkage rates reported in these latter two studies more closely approximated the rates we have observed in CFP-labeled microtubules in PtK2 cells (3.72 and 5.43 μm/min).

It is clear that the variability is great between cell types, and even from different laboratories working with the same cell type, i.e., PtK1 cells with shrinkage rates of 7.4 μm/min[26] and 19.8 μm/min.[21] In this case, the experiments were done six years apart, and it is possible that the passage numbers for the PtK1 cells used were substantially different. The many years of selection pressure *in vitro* could have resulted in physiological and genetic changes in the cells themselves. However, a large variation in depolymerization rates for spontaneously depolymerizing microtubules was observed between day-to-day measurements: 5.43 to 3.72 μm/min (Fig. 5). In addition, the microtubule location within the cytoplasm was shown to be a factor in the rate of depolymerization (see later discussion).

Classic UV laser-cutting experiments by Walker, Inoue, and Salmon have proposed a UV-activated mechanism to explain the rapid stabilization of the minus end.[15] Observations of ablated microtubules by both the near-IR femtosecond laser and 532-nm Nd:YAG laser are inconsistent with this theory, as they show the same stabilization as observed with the UV laser (Figs. 1 and 4). The stability of newly formed minus ends seems to be a characteristic of the microtubule itself rather than a mechanism dependent on laser wavelength.

Third, we observed a highly significant difference ($p \ll 0.01$) between average shrinkage rates of cut microtubules in the periphery of the cell (3.44 to 3.95 μm/min) compared to shrinkage rates of cut microtubules directly above or below the cell nucleus (13.66 μm/min). This observation may be relevant to differences in plus-end shrinkage rates observed in migrating newt cells when microtubules were either parallel to the leading edge of the cell (7.6 μm/min) or perpendicular to the leading edge (5.2 μm/min).[26] Our experimental results are consistent with these observations, and they may be explained by differences in the local structure and chemistry at the cell edge versus the nucleus. This is also consistent with recent studies that suggest stress fibers and the surrounding environment, specifically motor proteins and extracellular matrix components, can affect cytoskeletal dynamics.[6] Also, it is possible that the biomechanics and fluid mechanics within the cytoplasm are different between the thin lamellae regions of the cell, where single tubes are easily distinguished, and the thicker region around the nucleus, where the biochemical and biomechanical environments may be different. Notwithstanding these possible explanations, the statistical difference between depolymerization of cut microtubules at the periphery of the cell and above/below the nucleus is highly significant.

We have demonstrated that the near-IR femtosecond laser can be used for subcellular nanosurgery of individual microtubules in living cells. However, we have found no significant advantage of this laser over the picosecond green laser, or other lasers reported in the literature, for ablating single microtubules. In addition, the studies reported here have revealed several interesting observations on the dynamics of single microtubules, especially with respect to rates of depolymerization in different regions of the cell.

4 Materials and Methods

4.1 *Cell Culture*

Cell lines of rat kangaroo *Potorous tridactylis* (PTK2) originally obtained from the American Type Culture Center (ATCC) were used in these studies.[27] Stable cell lines expressing enhanced cyan fluorescent protein fused to alpha tubulin subunits were generated as described previously.[14] Cells were

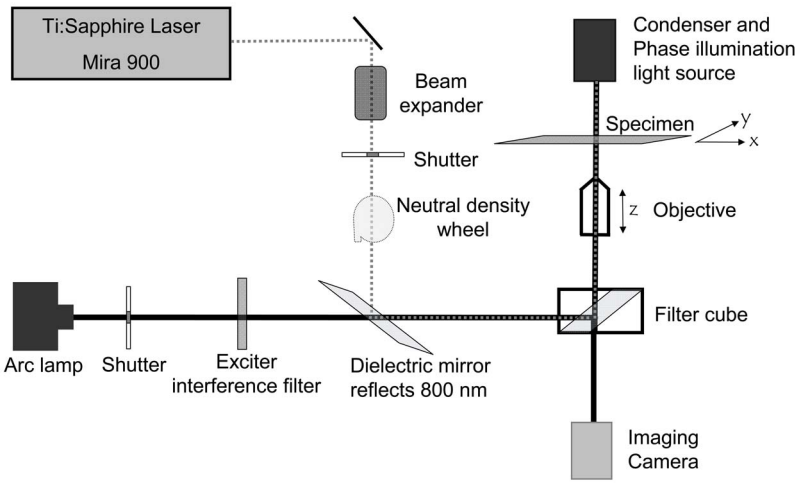

Fig. 7 Schematic diagram of imaging and laser ablation system. The Ti:sapphire laser beam is expanded and passes through a shutter and neutral density wheel before being directed through the microscope and objective. The beam is focused at the imaging plane. A dichroic mirror in the laser path reflects the beam and allows for fluorescence excitation light to transmit into the objective and illuminate the specimen.

thawed from frozen stock and grown to confluency before being seeded into Rose culture chambers at a density of 200,000 to 500,000 per chamber on glass coverslips. Culture media used was advanced MEM buffered with HEPES. The HEPES-buffered culture medium provided for a stable pH environment during the 30 min that the cells were removed from the incubator and placed on the microscope stage for laser irradiation. Under these conditions, cells grow normally in the Rose chamber and all stages of mitosis, prophase through cytokinesis, are observed during the 30 min of the experimentation as well as several hours beyond.

Cells used for immunofluorescence experiments were plated on coverglasses with etched grids (Bellco Glass, Vineland, New Jersey) to facilitate relocalization of targeted cells.

4.2 *Immunofluorescence*

Cells were fixed immediately after ablation with 2% paraformaldehyde and 3% glutaraldehyde in cacodylate buffer for a minimum of 15 min. Fixative was injected directly into the Rose chamber onstage to achieve immediate fixation. Cells were then incubated three times in 0.5-mg/ml $NaBH_4$ in phosphate buffered saline (PBS) (pH 8.0) for 10 min. Cells were washed in PBS three times and 0.1% Triton X-100 in PBS was added for permeabilization for 3 min. Cells were again washed three times in PBS. A mouse monoclonal anti-beta tubulin – Cy3 conjugated antibody (Sigma Company) was used at a 1:200 ratio in PBS with 1% BSA. Following a one-hour incubation period, cells were washed three times in PBS and mounted with aquamount onto a glass slide.

Cells were relocated using postirradiation digital images in combination with grid coordinates. Specific irradiated targets within the cells were determined via comparison to images acquired at the time of laser exposure. Fluorescent images were acquired at a 0.5-s exposure with a Cy3 filter cube (excitation 530 to 560-nm bandpass; dichroic mirror cut-on wavelength 570 nm; emission filter wavelength 573 tot 648 bandpass).

4.3 *Laser Ablation*

The femtosecond laser ablation system used is diagrammed in Fig. 7. A Coherent Mira 900 Ti:sapphire laser (Coherent Incorporated, Santa Clara, California) emitting 200 femtosecond pulses at 76 MHz was used for ablation at 800 nm. Laser power was controlled manually by a neutral density wheel, which allowed regulation of beam power from 0 to 700 mW. Laser power was measured by a FieldMaxII TOP power meter coupled to a PM3 probe (Coherent Incorporated, Santa Clara, California) with a 19-mm-diameter sensor. The probe was placed directly after the objective where the diameter of the laser beam was smaller than the sensor diameter. This allowed for collection of all light exiting the objective, which resulted in an estimate of the power level at the focal point of the specimen. The diameter of the laser beam at the focal point was calculated from the equation $d=1.22\lambda/\mathrm{NA}$, where λ is the wavelength and NA is a numerical aperture of the objective. Laser exposure time was controlled by a motorized Oriel (Stratford, Connecticut) electronic shutter controller, which allowed a minimum of 5-ms exposure time. Laser exposure times were set at 150 ms based on previously published work.[5] The laser beam was directed into the epi-illumination port (optics removed) of a Zeiss Axiovert S100 2TV microscope (Carl Zeiss Incorporated, Thornwood, New York) by a dichroic filter designed to pass visible arc lamp emission and reflect the 800-nm laser light. The beam was focused by a Zeiss $63\times$ PH3 oil immersion apochromat objective lens (numerical aperture 1.40). Initial microtubule dynamics experiments were conducted at a warm room temperature of 23 °C, and later experiments were conducted using an air stream stage incubator (Nevtec, Burnsville, Virginia) that maintained the cell culture medium at 34 °C. A comparison of the microtubule depolymerization rates at the two temperatures using the rank-sum statistical test showed that there was no difference in the rates between the two temperatures $p>0.95$. Thus, in this study the two groups are combined.

Targeting was accomplished by moving the stage (Ludl Incorporated, Hawthorne, New York) by joystick control until

the region of interest was positioned at the prealigned laser focal point. Laser ablation was accomplished by stage movement, such that the target region was exposed to the focused laser. Stage movement was controlled by a PCI-7344 motion controller and a MID-7604, 4 Axis Integrated Stepper Driver Power Unit (National Instruments), all controlled by our custom-made Robolase software.[28]

The picosecond laser ablation system used is described in detail by Botvinick and Berns.[28] The laser system was comprised of a 532-nm Spectra-Physics Vanguard laser with 76-MHz repetition rate and 80-ps pulse duration. Average power was attenuated by rotation of a neutral density wheel.

4.4 *Imaging*

Custom-coded LabVIEW software, Robolase, was used to control hardware and image acquisition.[28] Image acquisition occurred immediately before laser exposure, after laser exposure, and preselected sequential time points following ablation. 12 time series images were acquired at 5- to 7-s intervals. All controls for laser ablation and imaging are located on the Robolase control panel.

A 75-W mercury/xenon arc lamp was used to excite fluorescence. Exposure of the sample to excitation illumination was controlled by a motorized Oriel mechanical shutter and varied from 0.5 to 2 s. An external excitation interference filter (CFP bp 426 to 446 nm; YFP bp 490 to 510 nm) was used to select the excitation wavelengths. The microscope filter cube included a beamsplitter and emission interference filter (CFP dichroic long-pass 455 nm/emission 460 to 500 nm; YFP dichroic long-pass 515 nm/ emission 520 to 550 nm). Images were acquired using a Hamamatsu Orca C4742-95-12HR digital charge-coupled device (CCD) camera (Hamamatsu Corporation, Bridgewater, New Jersey). Images were stored as 16-bit tiff images.

The fluorescence excitation source for YFP experiments on the femtosecond laser was an X-Cite 120 Fluorescence Illumination System (Exfo Photonics Solution, Incorporated, Ontario, Canada). Exposure of the excitation source was controlled by Zeiss Axiovert 200M. Images were acquired using a Hamamatsu Orca-ER C4742-80 digital CCD camera.

4.5 *Microtubule Dynamics*

Microtubule depolymerization rates were calculated by playback of still and time sequence images (5 to 7-s intervals). A micrometer was used to determine micron:pixel ratios for calculation of depolymerization rates in microns/minute. Since the microtubule depolymerization rate data did not fit a normal Gaussian distribution, the nonparametric rank-sum statistical test was used instead of the Student's T-test. As with the T-test, the p value depicts the probability that the null hypothesis is true.

Acknowledgments

This work was supported by NIH grant R01 RR14892 and Air Force Office of Scientific Research grant F9620-00-1-0371.

References

1. A. Heisterkamp, I. Z. Maxwell, E. Mazur, J. M. Underwood, J. A. Nickerson, S. Kumar, and D. E. Ingber, Pulse energy dependence of subcellular dissection by femtosecond laser pulses," *Opt. Express* **13**(10), 3690–3696 (2005).
2. K. Konig, I. Riemann, P. Fischer, and K. J. Halbhuber, "Intracellular nanosurgery with near infrared femtosecond laser pulses," *Cell Mol. Biol. (Paris)* **45**(2), 195–201 (1999).
3. K. Konig, I. Riemann, F. Strucke, and R. LeHarzic, "Nanoprocessing with nanojoule near-infrared femtosecond laser pulses," *Med. Las. App.* **20**, 169–184 (2005).
4. W. Watanabe and N. Arakawa, "Femtosecond laser disruption of subcellular organelles in a living cell," *Opt. Express* **12**(18), 4203–4213 (2004).
5. L. Sacconi, I. M. Tolic-Norrelykke, R. Antolini, and F. S. Pavone, "Combined intracellular three-dimensional imaging and selective nanosurgery by a nonlinear microscope," *J. Biomed. Opt.* **10**(1), 14002 (2005).
6. S. Kumar, I. Z. Maxwell, A. Heisterkamp, T. R. Polte, T. P. Lele, M. Salanga, E. Mazur, and D. E. Ingber, "Viscoelastic retraction of single living stress fibers and its impact on cell shape, cytoskeletal organization, and extracellular matrix mechanics," *Biophys. J.* **90**(10), 3762–3773 (2006).
7. A. Vogel, J. Noack, G. Huttman, and G. Paltauf, "Mechanisms of femtosecond laser nanosurgery of cells and tissue," *Appl. Phys. B* **81**(8), 1015–1047 (2005).
8. S. La Terra, C. N. English, P. Hergert, B. F. McEwen, G. Sluder, and A. Khodjakov, "The de novo centriole assembly pathway in HeLa cells: cell cycle progression and centriole assembly/maturation," *J. Cell Biol.* **168**(5), 713–722 (2005).
9. T. M. Kapoor, M. A. Lampson, P. Hergert, L. Cameron, D. Cimini, E. D. Salmon, B. F. McEwen, and A. Khodjakov, "Chromosomes can congress to the metaphase plate before biorientation," *Science* **311**(5759), 388–391 (2006).
10. A. Khodjakov, R. W. Cole, and C. L. Rieder, "A synergy of technologies: combining laser microsurgery with green fluorescent protein tagging," *Cell Motil. Cytoskeleton* **38**(4), 311–317 (1997).
11. V. Magidson, F. Chang, and A. Khodjakov, "Regulation of cytokinesis by spindle-pole bodies," *Nat. Cell Biol.* **8**(8), 891–893 (2006).
12. J. Colombelli, E. G. Reynaud, J. Rietdorf, R. Pepperkok, and E. H. Stelzer, "In vivo selective cytoskeleton dynamics quantification in interphase cells induced by pulsed ultraviolet laser nanosurgery," *Traffic (Oxford, U. K.)* **6**(12), 1093–1102 (2005).
13. W. Tao, R. J. Walter, and M. W. Berns, "Laser-transected microtubules exhibit individuality of regrowth, however most free new ends of the microtubules are stable," *J. Cell Biol.* **107**(3), 1025–1035 (1988).
14. E. L. Botvinick, V. Venugopalan, J. V. Shah, L. H. Liaw, and M. W. Berns, "Controlled ablation of microtubules using a picosecond laser," *Biophys. J.* **87**(6), 4203–4212 (2004).
15. R. A. Walker, S. Inoue, and E. D. Salmon, "Asymmetric behavior of severed microtubule ends after ultraviolet-microbeam irradiation of individual microtubules in vitro," *J. Cell Biol.* **108**(3), 931–937 (1989).
16. K. Hughes, A. Forer, P. Wilson, and C. Leggiadro, "Ultraviolet microbeam irradiation of microtubules in vitro. The action spectrum for local depolymerization of marginal band microtubules in vitro matches that for reducing birefringence of chromosomal spindle fibres in vivo," *J. Cell. Sci.* **91**(4), 469–478 (1988).
17. M. W. Berns, *Biological Microirradiation: Classical and Laser Sources*, Prentice-Hall, Englewood Cliffs, NJ (1974).
18. A. Vogel and V. Venugopalan, "Mechanisms of pulsed laser ablation of biological tissues," *Chem. Rev. (Washington, D.C.)* **103**(2), 577–644 (2003).
19. P. T. Tran, R. A. Walker, and E. D. Salmon, "A metastable intermediate state of microtubule dynamic instability that differs significantly between plus and minus ends," *J. Cell Biol.* **138**(1), 105–117 (1997).
20. N. M. Rusan, C. J. Fagerstrom, A. M. Yvon, and P. Wadsworth, "Cell cycle-dependent changes in microtubule dynamics in living cells expressing green fluorescent protein-alpha tubulin," *Mol. Biol. Cell* **12**(4), 971–980 (2001).
21. E. Shelden and P. Wadsworth, "Observation and quantification of individual microtubule behavior in vivo: microtubule dynamics are cell-type specific," *J. Cell Biol.* **120**(4), 935–945 (1993).
22. L. Cassimeris, N. K. Pryer, and E. D. Salmon, "Real-time observations of microtubule dynamic instability in living cells," *J. Cell Biol.* **107**(6 Pt. 1), 2223–2231 (1988).
23. L. D. Belmont, A. A. Hyman, K. E. Sawin, and T. J. Mitchison, "Real-time visualization of cell cycle-dependent changes in microtubule dynamics in cytoplasmic extracts," *Cell* **62**(3), 579–589 (1990).

24. E. Schulze and M. Kirschner, "New features of microtubule behaviour observed in vivo," *Nature (London)* **334**(6180), 356–359 (1988).
25. C. M. Waterman-Storer and E. D. Salmon, "How microtubules get fluorescent speckles," *Biophys. J.* **75**(4), 2059–2069 (1998).
26. M. W. Berns, A. D. Floyd, K. Adkisson, W. K. Cheng, L. Moore, G. Hoover, K. Ustick, S. Burgott, and T. Osial, "Laser microirradiation of the nucleolar organizer in cells of the rat kangaroo (Potorous tridactylis). Reduction of nucleolar number and production of micronucleoli," *Exp. Cell Res.* **75**(2), 424–432 (1972).
27. M. W. Berns, J. Aist, J. Edwards, K. Strahs, J. Girton, P. McNeill, J. B. Rattner, M. Kitzes, M. Hammer-Wilson, L. H. Liaw, A. Siemens, M. Koonce, S. Peterson, S. Brenner, J. Burt, R. Walter, P. J. Bryant, D. van Dyk, J. Coulombe, T. Cahill, and G. S. Berns, "Laser microsurgery in cell and developmental biology," *Science* **213**(4507) 505–513 (1981).
28. E. L. Botvinick and M. W. Berns, "Internet-based robotic laser scissors and tweezers microscopy," *Microsc. Res. Tech.* **68**(2), 65–74 (2005).